20

Waste Gas Treatment Using Zeolites in Nuclear-Related Industries

Jun Izumi
Mitsubishi Heavy Industries, Ltd., Nagasaki, Japan

I. INTRODUCTION

Urgent requirements exist in nuclear related industries for the development of high-efficiency processes for waste gas treatment. While mainly distillation and absorption methods have been used in the past, adsorption processes have recently begun to be adopted. A summary of waste gas treatment processes that feature adsorption are shown in Table 1 (with Refs. 1–7).

From the process point of view, temperature swing adsorption (TSA) and pressure swing adsorption (PSA) have contributed greatly to the development of gas separation methods (8). In TSA, adsorption of weak adsorbates occurs at a lower temperature with subsequent desorption at a higher temperature. In PSA, adsorption of weak adsorbates occurs at higher pressures and is followed by desorption at a lower pressure. In terms of adsorbents, performance improvements of zeolites and activated carbons are important. This chapter provides a specific example of zeolite application, i.e., xenon purification using vacuum pressure swing adsorption (VPSA), which delivers the lowest energy consumption among various PSA operations.

II. WASTE GAS TREATMENT PROCESSES

A. Xenon Purification from Radioactive Krypton

1. Introduction

Xenon is an inert gas that is important in industrial applications such as seal gases for electric discharge lamps, contrast media for medical treatment, and working fluids for gas turbines and ionic propulsion. Since air contains 0.1 ppm xenon, the conventional process for producing xenon is through cryogenic separation as a byproduct of oxygen and nitrogen production (9).

Because trace recovery of xenon from air is very expensive, its use is currently limited to specialty purposes, despite xenon's unique and remarkable properties. However, large amounts of xenon are released as fission products from the dissolving process of spent nuclear fuel (10). When radioactive krypton (Kr-85) is removed using cryogenic separation, xenon is enriched up to 99 vol %, as shown in Fig. 1 (9). Nevertheless, because this

Table 1 Waste Gas Treatment Processes Featuring Adsorption on Zeolites

Application	Process	Type of zeolite	Present status	Ref.
Iodine removal from light-water reactors and reprocessing facilities	Iodine removal	Ag-X Ag-mordenite	Commercialized	1,2
Iodine fixation for long-term storage	Iodine fixation	Iodine adsorbed zeolite/apatite	R&D stage	3
Krypton removal from reprocessing facilities	TSA, PSA	Ag-dealuminated natural mordenite	R&D stage	4,5,21
Xenon purification at reprocessing facilities	PSA	Na-X	R&D stage	6
NOx removal and recovery from reprocessing facilities	TSA, PSA	Silicalite	R&D stage	7
Tritium removal	TSA, fixation	Na-A	R&D stage	22
NOx, ozone removal from accelerator	Adsorptive reactor	Silicalite	Commercialized	17

xenon contains a small amount of Kr-85, the radioactive level of which is higher than permissible, it cannot be used in general industrial applications. If an appropriate Kr-85 removal technique could be developed, the xenon supply situation would be greatly improved. Accordingly, Kr-85 removal from xenon-enriched gas has been studied, and PSA has been identified as one of the most likely candidate processes (13). This is because of the priorities placed on high levels of decontamination, the practicality of remote operation, and the release of almost no radioactive waste.

Low-temperature experimentation to purify xenon using TSA was studied in the 1980s (11), and high-temperature experimentation featuring PSA was conducted recently

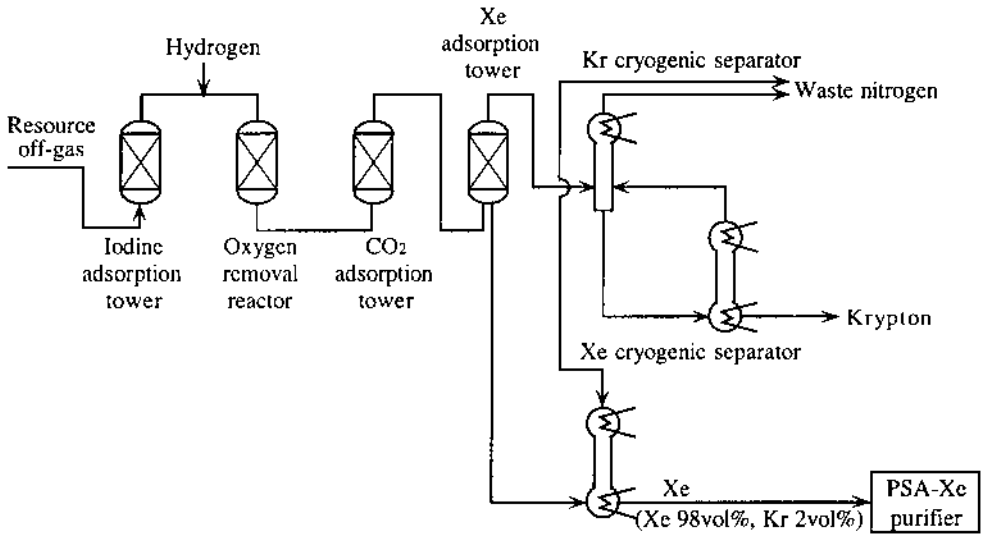

Fig. 1 Schematic illustration of radioactive off-gas treatment. (From Ref. 9.)

(13). In this chapter, adsorbent selection, a schematic illustration, and design performance are introduced, along with other relevant topics.

2. Adsorbent Selection

In a xenon–krypton binary system, the amount of xenon adsorbed on any kind of zeolite is commonly greater than that of krypton at the equilibrium condition. The greater the xenon separation factor α_x, the more preferable the xenon adsorbent for PSA. Here, the separation factor α_x is defined by Equation (1):

$$\alpha_x = (q_x/C_x)/(q_k/C_k) \tag{1}$$

where q is the amount adsorbed at the equilibrium condition, C is the adsorbate concentration, x is xenon, and k is krypton (6).

As shown in Fig. 2a, the sequence of the amount of xenon adsorbed (from greater to smaller) is Na-X type zeolite (Na-X), Ca-X type zeolite (Ca-X) > Ca-A type zeolite (Ca-A) > Na-mordenite. Also, as shown in Fig. 2b, in the region of higher krypton concentration, the sequence of the amount of krypton adsorbed is the same sequence as for xenon. In the region of lower concentration, however, the sequence changes to Ca-A > Ca-X > Na-mordenite, Na-X. For xenon adsorbent, given the desirability of a larger amount of adsorbed xenon and a smaller amount of krypton (resulting in the higher xenon separation factor α_x shown in Fig. 2c), Na-X is deemed to be the most suitable adsorbent for xenon purification using PSA (6).

The amount of dynamically absorbed xenon q_x on Na-X reaches its maximal value at room temperature, and decreases at both lower and higher temperatures. Since the amount of adsorbed xenon increases at lower temperatures at the equilibrium condition, the xenon adsorption rate is considered to decrease at lower temperatures. With respect to the xenon separation factor α_x, since Ca-X is capable of maintaining a higher value, Na-X and Ca-A exhibit maximal values at room temperature.

Although the xenon separation factor α_x under binary conditions is one of the most important criteria in selecting the adsorbent for PSA-xenon purification, it has a tendency when measured under binary conditions to give a different value from that assumed under the monocomponent conditions of xenon and krypton. Thus, if possible, direct measurement of the xenon separation factor under binary conditions is desirable.

3. Xenon Purification PSA

a. Single-Stage Apparatus

The authors have designed, manufactured, and tested a xenon purification apparatus that features single-stage VPSA at the bench scale (6); a schematic illustration is shown in Fig. 3. In this experiment, following the adsorption of xenon by means of a xenon adsorption tower in the xenon–krypton binary system, coadsorbed krypton is purged with the parallel flow of the product xenon from the bottom of the tower, prior to desorption for the recovery of the enriched (or decontaminated) xenon. The cold test (using natural krypton) has been completed, and a hot test (using radioactive krypton) is planned.

b. Xenon Purification Performance

Impurity removal at the adsorption stage has been widely used for water vapor removal, hydrogen purification, oxygen production (removal of nitrogen), solvent recovery, etc. Particularly in the case of PSA-hydrogen purification, impurities of 10 vol % can be easily removed to a level of less than 1 ppm. On the other hand, the above-mentioned parallel

A)

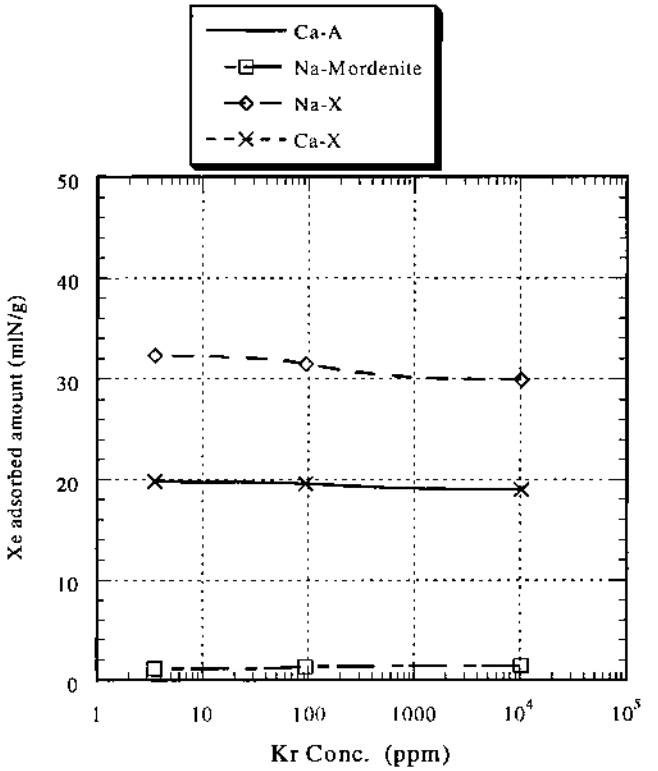

B)

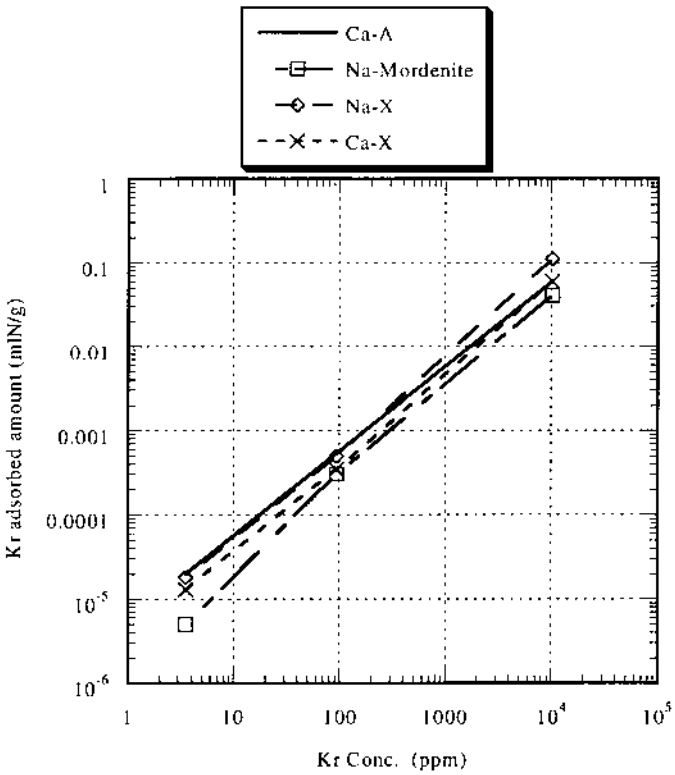

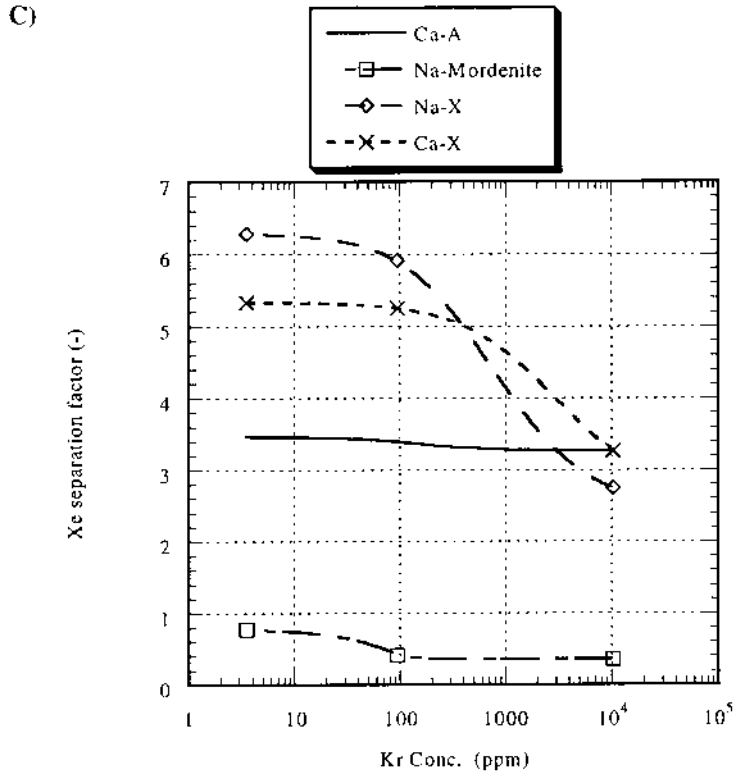

Fig. 2 (A) Kr concentration and Xe adsorbed amount, (B) Kr concentration and Kr adsorbed amount, and (C) Kr concentration and Xe separation factor (all under Kr-Xe binary conditions). (From Ref. 6.)

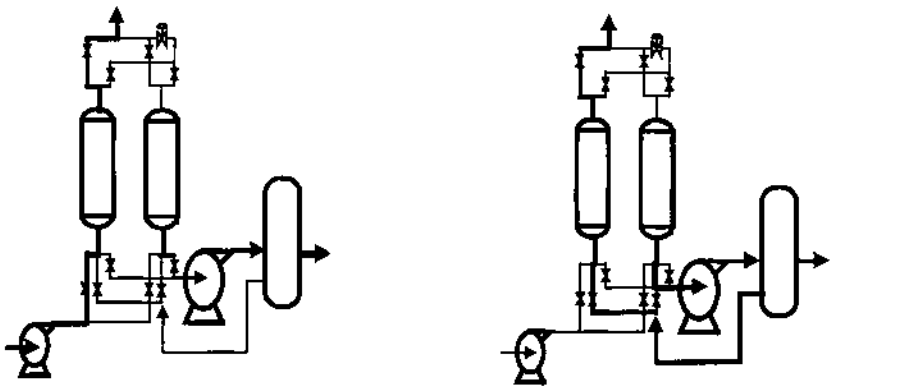

Fig. 3 Kr enrichment with a parallel purge at a description stage. (From Ref. 6.)

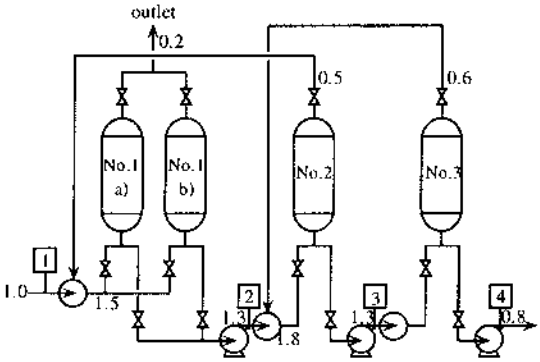

	1	2	3	4
	Inlet	1st stage outlet	2nd stage outlet	3rd stage outlet
Flow rate	1.0	1.3	1.3	0.8
Kr conc.	10^{-2}	10^{-7}	10^{-12}	10^{-17}
Radioactivity	11	10^{-4}	10^{-9}	10^{-14}

Fig. 4 Schematic illustration of PSA xenon purification process. (From Ref. 6.)

flow purge process is used for the enrichment of adsorbates such as in CO recovery, nitrogen production using nitrogen adsorbent, CO_2 recovery, and SO_2 recovery.

In the case of xenon purification in a xenon–krypton binary system (krypton concentration of 1–10,000 ppm), since the xenon separation factor α_x of Na-X is 6, it was confirmed that the maximal krypton decontamination factor reaches 10^3 at a purge ratio of 70% and 10^4 at a purge ratio of 80%. The purge ratio R is defined by Eqs. (2) and (3).

$$R = [\text{parallel purge flow rate}]/[\text{desorption gas rate}] \quad (2)$$

$$[\text{Product gas rate}] = [\text{desorption gas rate}] - [\text{parallel purge flow rate}] \quad (3)$$

Based on the experimental results of the single stage xenon purification unit, the actual xenon purification process, featuring a cascade enrichment system, can be designed. According to our assumptions, radioactive krypton (10^6 Bq/cm^3) can be removed to a natural level (10^{-19} Bq/cm^3) using a VPSA-xenon enrichment process with three stages. A schematic illustration of the cascade xenon enrichment system (6) is shown in Fig. 4.

Specific electric power consumption for the removal of radioactive krypton is assumed to be 5.5 kWh/m^3 N, which would purify xenon at an extremely low-energy cost in comparison with the current market price of xenon. The loading capacity [recovered gas rate (m^3 N/h) per ton of xenon adsorbent] to purify xenon is estimated to be 200–240 m^3 N h^{-1} ton^{-1} for each stage.

The features of the VPSA–xenon process described above can be summarized as follows:

1. As the only inputs are electricity and cooling water, very little radioactive waste is generated.
2. The decontamination factor for each stage is very high.
3. The system is automatically operated.

VPSA-xenon is therefore one of the most suitable processes for the removal of radioactive krypton, which requires a high decontamination factor in the trace amount region.

B. Radioactive Iodine (I-129) Fixation to Zeolite Dispersed with Apatites

1. Introduction

Although there is the probability of emissions of trace amounts of short half-life radioactive iodine from light-water reactors (LWRs), they are removed by the activated carbon

adsorption bed known as a charcoal filter. This iodine adsorption is mainly used for a decay of the short half-life radioactive iodine to below the permissible radioactivity level to extend the residence time of the iodines in the charcoal filter. This filter serves to remove the short half-life radioactive iodine but is not sufficiently functional to remove long half-life iodine I-129.

Because of its long half-life (17 million years) and the low retardation effect expected by engineered and natural barriers, I-129 is the most influential nuclide for exposure dose evaluation in TRU waste disposal. For the removal of I-129 from reprocessing facilities with a high removal ratio [decontamination factor (DF) > 100] and stable fixation, inorganic porous media containing Ag, such as Ag-X type zeolite (Ag-X), Ag-mordenite, and Ag-silica gel (Ag-S), have been used (1,2).

In particular, as the amount of irreversibly adsorbed iodine on zeolites is substantial, use of such zeolites has recently been on the increase. Although studies have demonstrated the fixation of I-129 for long periods with (a) glass (12), (b) copper (19), (c) sodalite (14), etc., there is no technology that currently satisfies the requirements posed by extremely long-term storage of more than 1 million years. In this chapter, iodine fixation using a hot press of the iodine–adsorbed zeolite that is dispersed into an apatite matrix is introduced.

2. Iodine Adsorption on Zeolite

For iodine removal with a high DF value (DF > 100) in the off-gas of reprocessing facilities, a large amount of adsorbed iodine and strong irreversibility are required (3). The amounts of adsorbed iodine corresponding to (a) Na-X type zeolite (SiO_2/Al_2O_3 ratio 2.5), (b) Ca-X type zeolite, (c) Ag-Na-X type zeolite, (d) Ag-Ca-A type zeolite, (e) ALPO, and

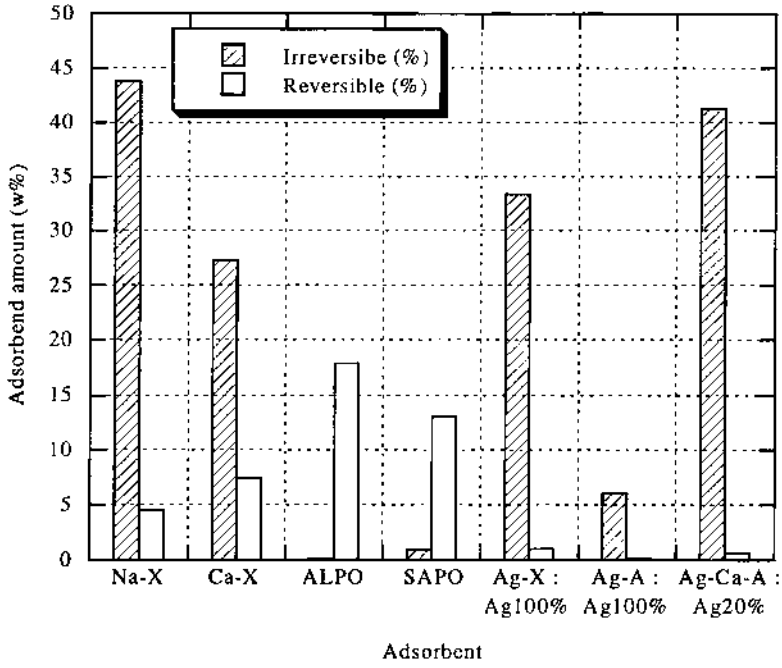

Fig. 5 Iodine adsorbed amount on zeolites; adsorption temperature 298K, I_2 concentration 1,000 ppm (no water vapor). (From Ref. 3.)

(f) SAPO are shown in Fig. 5 (3). Because the Ag ion is exchanged into the zeolite, the irreversibility of the iodine adsorption increases greatly. Upon Ag ion exchange and I adsorption, it is assumed that Ag-I bonds are formed inside the zeolite crystal.

Ag-X and Ag-Z have been used as iodine adsorbents at reprocessing facilities. Ag-Na-A zeolite, in which the diameter of the pore window is smaller than that of the iodine molecule, shows little adsorbed iodine uptake. This is because, for Na-A, the Na ions block the eight-membered ring windows and the entry is restricted to 4 Å. On the other hand, a Ca-A zeolite with 20% of the Ca ions exchanged with Ag ions (Ag-Ca-A) has a large amount of irreversibly adsorbed iodine. Upon exchange of the Na ions by Ca ions, the zeolite pore opening widens to 5 Å. This is because the Na ions, which were located at the windows, are now gone and the Ca ions are located within the zeolite cages (not blocking the window). Zeolites take up twice as much Na as Ca. Upon exchange of Na ions with Ca ions, the accessible window diameter is larger than the molecular diameter of iodine (I_2), and iodine penetrates into the zeolite and is strongly adsorbed at the active Ag ion adsorption site. ALPO and SAPO display no irreversible adsorption of iodine. Although these adsorbents cannot be used for iodine fixation, they are expected to be useful as PSA-iodine adsorbents.

3. Apatite Matrix Formation

Inorganic porous media that are used for radioactive iodine removal need to be stored indefinitely. Given that extremely long-term storage technology has not been established, several processes are being studied. For long-term storage, the basic requirements for economical storage are as follows: (a) the fixation body shows extremely low solubility in contact with ground water for more than 1 million years, and (b) the fixation body contains a substantial amount of iodine. The fixation bodies currently being studied, such as glass, cement, copper, apatite, and sodalite, cannot satisfy these two conditions. Although

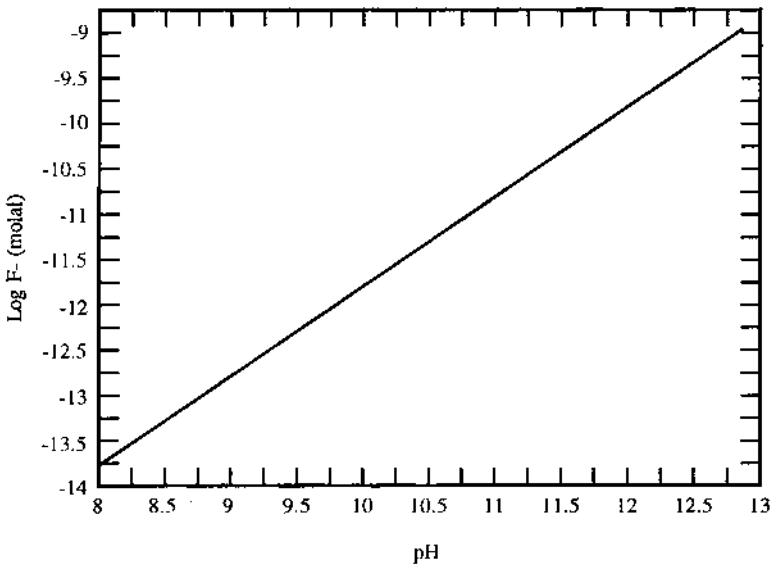

Fig. 6 Calculated solubility of fluorapatite [$Ca_5(PO_4)_3F$] in 0.01 molal NaCl at 25°C and 1 bar. (From Ref. 20.)

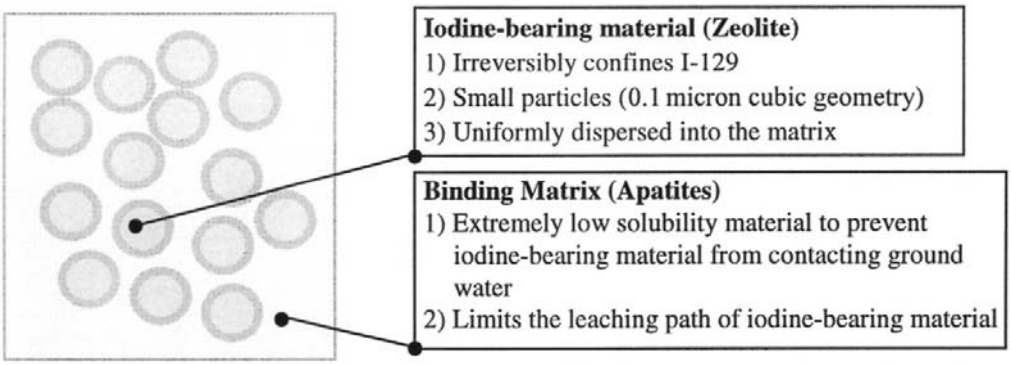

Fig. 7 Concept of multilayered distributed waste form for I-129. (From Ref. 3.)

Ag-exchanged zeolite shows a large amount of adsorbed iodine, it releases iodine after relatively brief contact with water. On the other hand, fluoroapatite (FAP) exhibits an extremely low solubility, as shown in Fig. 6 (20).

FAP is therefore one of the leading candidates for the matrix material (15). For forming, an iodine-adsorbed zeolite crystal is dispersed into FAP powder and compressed at 200 kg/cm^2. The formed medium is calcined at 1200 K for about 10 min by means of spark plasma sintering, allowing the removal of micropores and the formation of a high-density iodine fixation material (95% or greater) without a loss of adsorbed iodine. As this iodine fixation medium contains FAP, which is among the lowest solubility inorganic compounds in existence and is used for the matrix material, iodine can be expected to remain fixed for a few million years. A conceptual illustration of the iodine fixation body featuring FAP is shown in Fig. 7 (3). The fixation conditions of the iodine-adsorbed zeolite dispersed into FAP and the specifications of the fixation body are shown in Table 2.

C. NOx and Ozone Removal from Accelerator Work Areas Using High-Silica Zeolite

1. Introduction

NOx and ozone, which are generated by β and γ rays leaked from accelerators, must be removed from the immediate work area in order to maintain the local environment (16).

Table 2 Specification of Fixation Body

Adsorbent	Ag-X, Ag-Z, Ag-Ca-A
Matrix	FAP
Iodine adsorbed amount	42 g–I_2/100 g-ads.
Adsorbent/matrix ratio (w/w)	20:80
Foaming process	SPS
Foaming pressure	50–90 MPa
Foaming temperature	1100–1400 K
Density of fixation body	3.2 g/cm^3
Void ratio of fixation body	$<0.1\%$

Source: Ref. 2.

Although activated charcoal has been used conventionally for this purpose, it cannot remove NO; in addition, it is consumed by ozone.

When the authors studied a chemical reaction between NO and ozone on several kinds of zeolite (X, Y, USY, silicalite, etc.), it was found that NO and ozone could be reacted to form nitric acid on USY and that it could be completely fixed (17). Since the NO homogeneous oxidation reaction in the gas phase is very slow at NO concentrations of less than 10 ppm, this rapid oxidation reaction of NO on USY is quite remarkable. Our understanding of this reaction is that (a) NO and ozone are first coadsorbed and enriched on USY; (b) the following NO oxidation reactions then proceed very rapidly: $NO + O_3 \Rightarrow NO_2 + O_2$, $2NO_2 + O_3 \Rightarrow N_2O_5 + O_2$, $N_2O_5 + H_2O \Rightarrow 2HNO_3$; and (c) HNO_3 is fixed on USY as the adsorbate.

A bench scale test of NOx and ozone removal featuring this adsorptive chemical reaction was undertaken (17). Experimental conditions consisted of: (a) gas composition of NO 1–20 ppm, O_3 1–40 ppm, and H_2O 5000–50,000 ppm; (b) inlet gas rate of 40 m^3 N/h; (c) temperature of 283–313 K; (d) SV values of 5000–35,000 L/h; and (e) test pieces for anticorrosive (HNO_3) metal selection exposed in process streams. This process was scaled up to a practical level, and it has been used for NOx and ozone removal from a circulation stream of about 8000 m^3 N/h in the work area of an accelerator.

2. Adsorbent Evaluation

Figure 8 shows an experimental apparatus to evaluate the adsorptive reaction between NOx and ozone (17). First, NO was added to humid air (H_2O 2.5 vol %), after which ozone generated using an ozone generator was added to this air and its chemical composition was adjusted to specified concentrations (NO 3 ppm, O_3 24 ppm, H_2O 2.5 vol %). This gas was supplied to a small column loaded with 5 g of adsorbent. In the small column, chemical reactions (a)–(c) proceeded under water vapor until NO was finally converted to nitric acid: (a) $NO + O_3 \Rightarrow NO_2 + O_2$, (b) $2NO_2 + O_3 \Rightarrow N_2O_5 + O_2$, (c) $N_2O_5 + H_2O \Rightarrow 2HNO_3$.

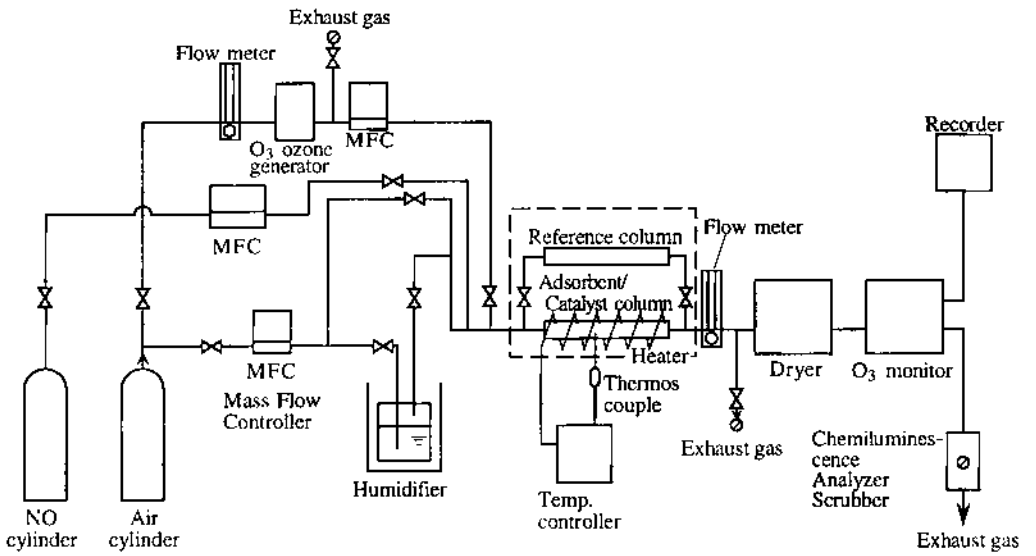

Fig. 8 Adsorbent/catalyst reaction apparatus. (From Ref. 17.)

Since nitric acid is an extremely strong adsorbate and is completely adsorbed on the adsorbent, only NOx ($NO + NO_2$) and nonreacted ozone pass through from the outlet of the column. At the outlet, ozone was measured with a nondispersive UV absorbance monitor and NOx was measured with a chemiluminescence analyzer. This was followed by NOx to NO conversion with a converter. The experimental conditions are shown in Table 3.

Figure 9 shows the time dependencies of the outlet NOx and ozone concentrations during the 200 h adsorptive reaction (17). When USY (SiO_2/Al_2O_3 ratio = 70) was loaded, the ozone concentration rose to 0.1 ppm in 25 h, and this value was maintained for 200 h. NOx could not be detected during this time, indicating that the NOx was entirely converted to nitric acid. Since the outlet NOx concentration remained at 1 ppm without USY (the remaining 2 ppm was nitric acid), it was confirmed that the NOx–ozone reaction was greatly accelerated on USY.

When silicalite was loaded, the outlet ozone concentration was 0.08 ppm and the NOx concentration increased gradually to reach 0.07 ppm in 200 h. Since silicalite is a high-silica zeolite (SiO_2/Al_2O_3 ratio = 400), the performance of NO to nitric acid conversion was not particularly high. It was assumed that some portion of the ozone was decomposed on silicalite but that it was not sufficient to realize a high conversion ratio. In the case of Na-Y, the outlet ozone concentration remained at 0.002 ppm and substantial ozone decomposition on Na-Y was measured. The outlet NOx concentration increased rapidly and reached 0.25 ppm in 200 h. Because of the substantial ozone decomposition, the yield of nitric acid was low and the weak NO_2 adsorbate passed through quickly. In the case of Na-X, ozone could not be detected at the outlet, whereas the outlet NOx concentration increased most rapidly, and Na-X showed the lowest nitric acid yield. When the SiO_2/Al_2O_3 ratio of faujausite crystals increased, it was confirmed that ozone decomposition was avoided and that the performance of the NO to nitric acid conversion was improved.

When the NOx and ozone reactions proceeded on USY, it appeared that the reactions could be accelerated because of their adsorption and enrichment to USY crystals, and that the converted nitric acid could be effectively fixed to USY. Because USY is strongly hydrophobic, it can adsorb NOx and ozone simultaneously, and it can convert NOx to nitric acid effectively even under high water vapor concentrations. Since

Table 3 Experimental Conditions of NOx-O_3 Adsorptive Reaction

Adsorbent	a) USY b) Silicalite c) Na-Y d) Na-X
Inlet gas rate	5 l N/min
Inlet NO conc.	3 ppm
Inlet O_3 conc.	24 ppm
Inlet H_2O vapor	1.8 vol%
Adsorption temp.	25°C
Adsorption period	200 h
Monitoring items	Outlet NOx, ozone conc.

Source: Ref. 17.

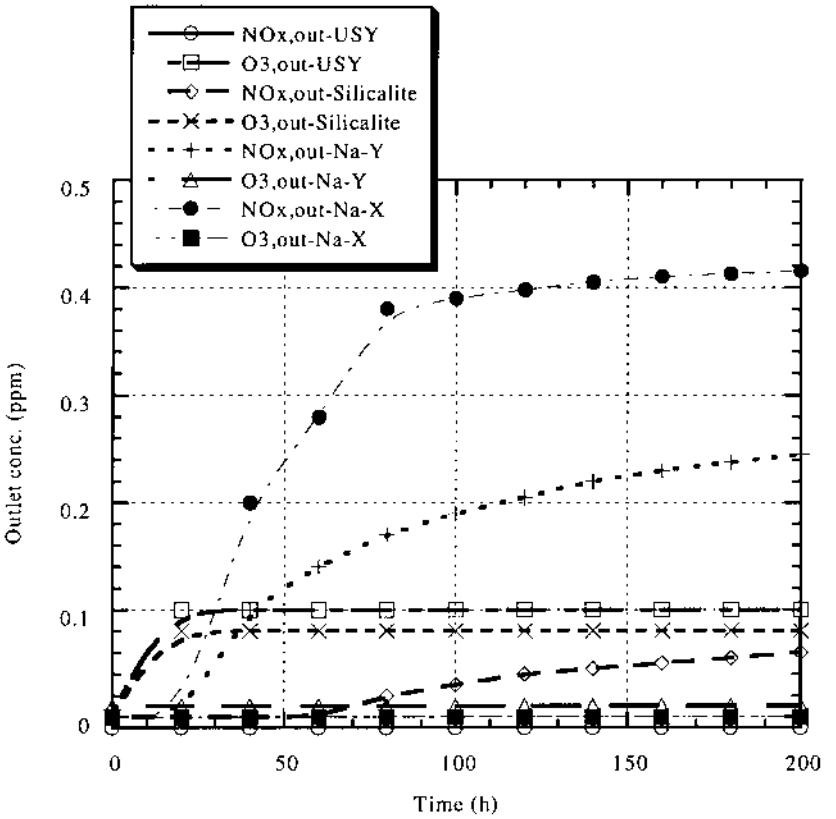

Fig. 9 Time dependency of outlet concentration of NOx and ozone through different zeolite adsorbents. (From Ref. 17.)

USY has little aluminum, it shows strong acid resistance and is destroyed by the fixed nitric acid. Also, it can be regenerated by heating to remove nitric acid.

3. Ozone Decomposer

As stated in Sec. II, nonreactive ozone passes through the adsorptive reaction column filled with USY. To remove ozone, an ozone decomposer, which was filled with ozone decomposition catalyst, was installed in the immediate downstream of the NOx adsorptive reactor. A Pt-Cu-Cr catalyst (Nissan Girdler Catalyst Co., pellet size; 1/16 in., SV; 30,000) was used.

III. ACTUAL NOx AND OZONE REMOVAL PROCESS

A. Apparatus and Procedure

Since the specifications of the NOx adsorptive reactor and ozone decomposer had been determined, NOx conversion to nitric acid and ozone decomposition performance were evaluated using a bench scale apparatus with 40 m^3 N/h inlet gas. A schematic illustration of the bench scale apparatus is shown in Fig. 10 (17). Concentrations of 3 ppm NO and 24 ppm ozone were added to circulation gas from a dummy cylinder simulating the work area

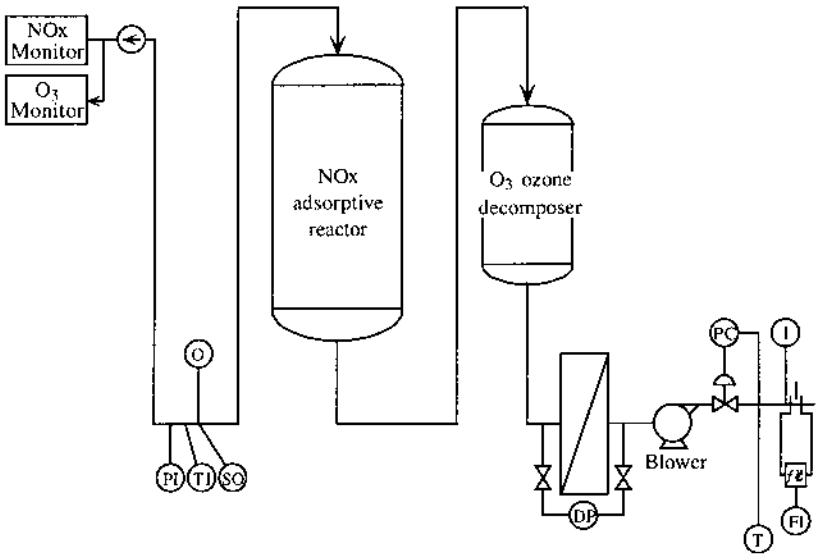

Fig. 10 Schematic illustration of NOx and ozone removal process. (From Ref. 17.)

of an accelerator. The relative humidity was adjusted to 60% at 25°C and supplied to the NOx adsorptive reactor, which was loaded with 1-L USY honeycombs.

Figure 11a shows the outlet/inlet NOx ratio and the outlet/inlet ozone ratio under conditions of room temperature, an inlet gas rate of 40 m^3 N/h (NOx adsorptive reactor SV value: 10,000), 60% relative humidity, O_3/NOx ratio = 8, and NOx concentration between 0.35 and 3.2 ppm. (For reference, the outlet/inlet NOx ratio and ozone ratio without adsorbent under the same conditions are shown in the same figure). When the inlet NOx concentration increased, the outlet/inlet NOx ratio became smaller. It was assumed that the NOx-O_3 reaction rate on USY became faster at higher concentrations. Without USY, such a low outlet/inlet NOx ratio could not be realized. It was understood that USY could adsorb ozone without decomposition when it adsorbed NOx; NOx and ozone were enriched on USY and the NOx-O_3 reaction rate increased.

Figure 11b shows the outlet/inlet NOx ratio and the outlet/inlet ozone ratio under the conditions of room temperature, an inlet gas rate of 40 m^3 N/h (NOx adsorptive reactor SV value: 10,000), 60% relative humidity, 3 ppm NOx, and with the O_3/NOx ratio varied between 1.5 and 7.5. When the O_3/NOx ratio increased, the outlet/inlet NOx ratio became much lower (17). When the NOx-ozone reaction on USY was compared with that without USY, the outlet/inlet NOx ratio on USY (particularly in the lower O_3/NOx ratio region) showed a much smaller value. That is, USY accelerated the NOx-O_3 reaction remarkably. Since it was confirmed that the high NOx removal ratio (even in the lower NOx concentration region) was realized with the NOx-O_3 adsorptive reaction on USY, this reaction could prove highly advantageous in removing NOx and ozone completely from the work space of accelerators.

Figure 11c shows the outlet/inlet NOx ratio and the outlet/inlet ozone ratio under conditions of room temperature, an O_3/NOx ratio = 1.5, 60% relative humidity, 3 ppm NOx, and inlet gas rate varied between 10 and 40 m^3 N/h (NOx adsorptive reactor SV value: 2500–10,000). When the inlet gas rate increased, the outlet NOx/O_3 ratio became greater (17). The outlet/inlet NOx ratio using USY was much lower than that without

A)

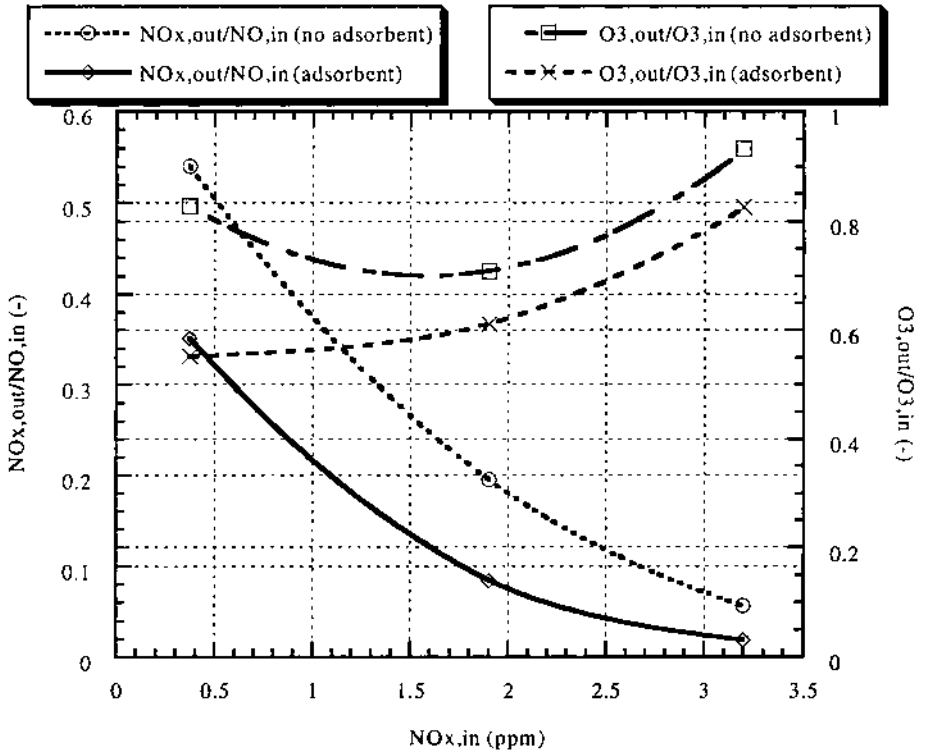

B)

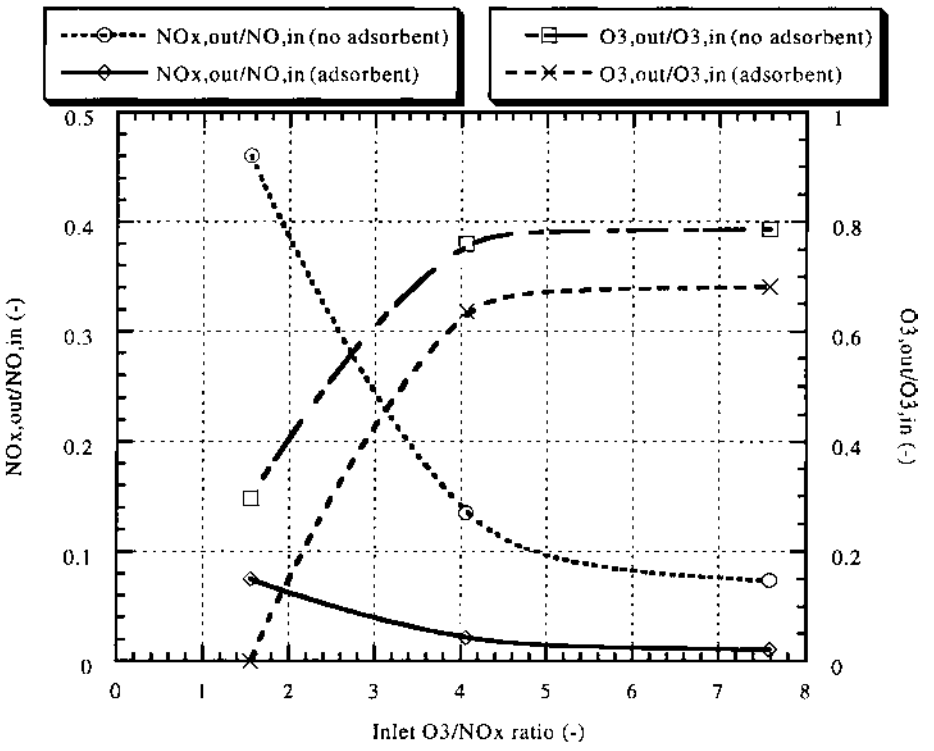

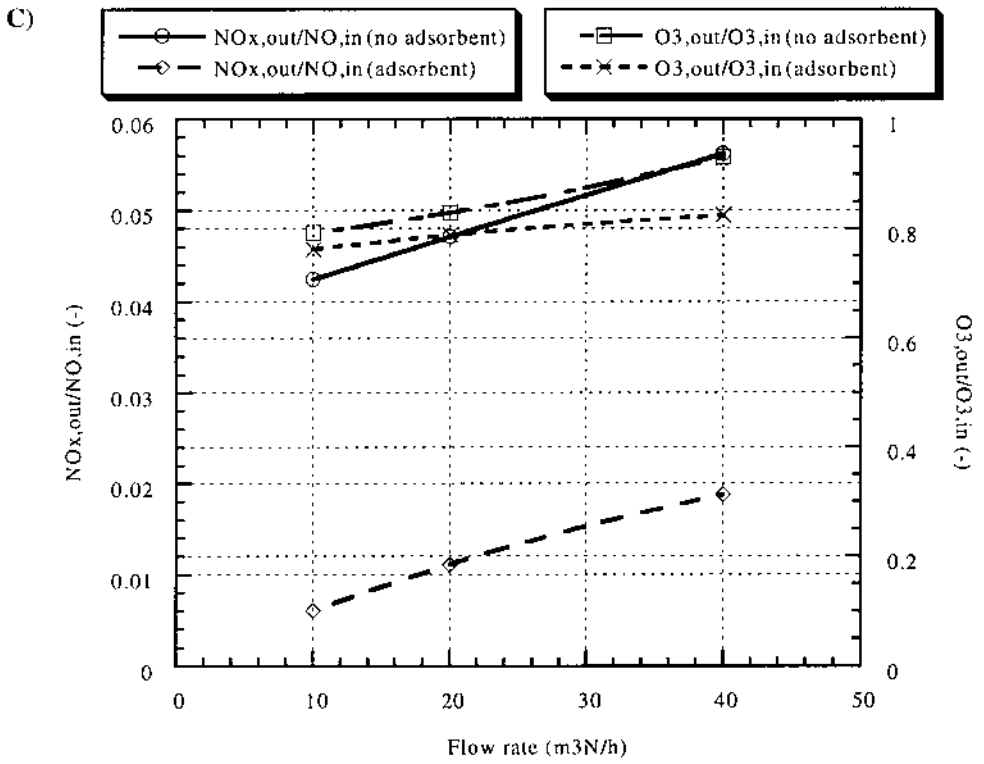

Fig. 11 (A) Relationship between inlet NOx concentration and outlet NOx and ozone removal ratio (temp. = 25°C, RH = 60%, flow rate = 40 m^3N/h). (B) Relationship between inlet O_3/NOx ratio and outlet NOx and ozone removal ratio (temp. = 25°C, RH = 60%, flow rate = 40 m^3N/h, NOx = 3 ppm). (C) Relationship between flow rate and outlet NOx and ozone removal ratio. (From Ref. 17.)

USY. Considering conventional processes such as selective contact reduction (NH_3-NOx reaction at 300–500°C) and the Nox-absorption process, the outlet/inlet NOx ratio of 0.07 at SV 10,000 in the lower concentration region featuring NOx-O_3 adsorptive reaction on USY as observed in this study was remarkable. Because ozone was decomposed at an SV value of 30,000 with Pt-Cu-Cr honeycomb as the ozone decomposer, no ozone could be detected and the high stability of this unit was confirmed.

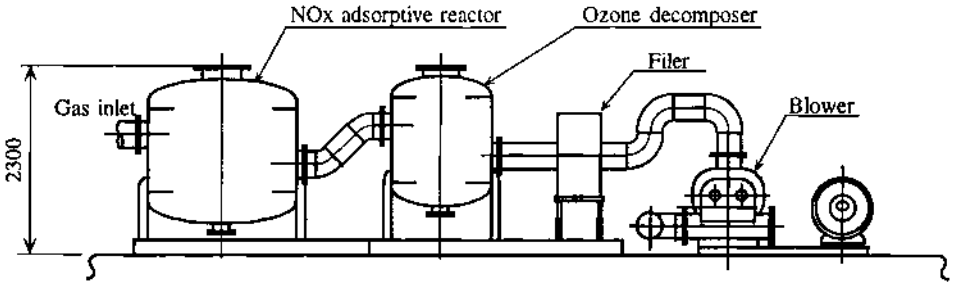

Fig. 12 Bird's eye view of the NOx/O_3 removal unit. (From Ref. 17.)

Table 4 Specifications of NOx/Ozone Removal Unit

NOx adsorptive reactor	Adsorbent	USY
	Adsorbent amount	1.7 ton
	Tower shape	1.86 m I.D. × 0.95 m height
Ozone decomposer	Catalyst	Pt-Cu-Cr
	SV value	10^4 m^3/m^3
	Catalyst amount	0.89 m^3
	Tower shape	1.3 m I.D. × 0.9 m height
Blower	Type	Turbo fan
	Circulation flow rate	9,900 m^3/h
	Outlet pressure	700 mm aq. Max.
	Motor power	50 kW

Source: Ref. 17.

Table 5 Material Balance of NOx/Ozone Removal Unit

	Line	0	1
Gas composition (–)	NOx	3×10^{-6}	2×10^{-8}
	O_3	24×10^{-6}	2×10^{-8}
	H_2O	0.018	0.018
	Air	0.972	0.972
	Total	1.00	1.00
Flow rate (m^3/N)	NOx	0.024	0.00016
	O_3	0.194	0.00016
	H_2O	146.0	146.0
	Air	7,950	7,950
	Total	8,096.218	8,096
Temp. (°C)		25	28
Pressure (Pa)		0.0995	0.102

Source: Ref. 17.

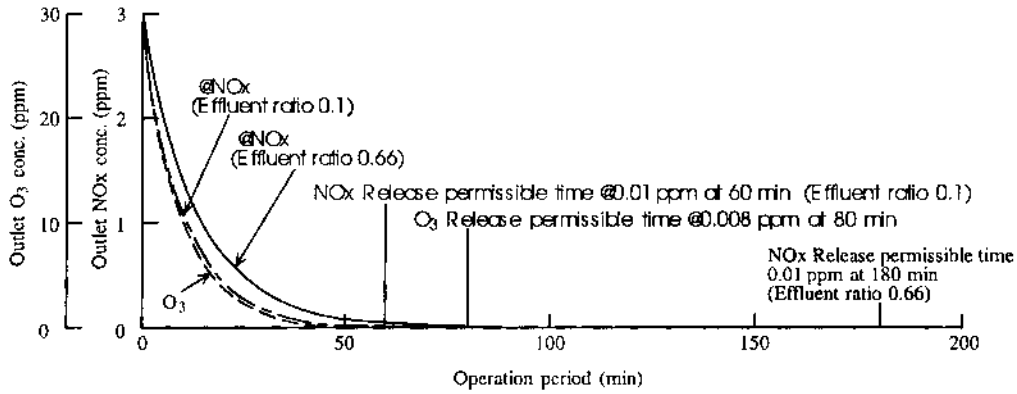

Fig. 13 Time dependency of NOx and ozone concentrations in a work space after stoppage. (From Ref. 17.)

IV. ACTUAL UNIT OPERATIONS

Based on the findings described above, an NOx and ozone removal unit for an accelerator (NOx of 3 ppm, ozone of 24 ppm, inlet gas rate of 8000 m^3N/h) was designed and fabricated (17). The unit is displayed in Fig. 12 and Tables 4 and 5 show its specifications. Figure 13 shows one of the results of the time dependency of NOx and ozone concentrations in a work space after stoppage of an accelerator (17). (Actual plant operation started in the latter part of 1999.) At 30 min after a stoppage, NOx and ozone concentrations were confirmed to be below the target value of 0.04 ppm.

REFERENCES

1. S Matsuoka, H Nakamura, T Tamura, T Takano, Y Ito. J Nucl Sci Technol 21: 862–870, 1984.
2. T Kanazawa, T Fujii, I Nakai. Research and Development (Kobe Steel, Ltd), 31: 73–76, 1981.
3. J Izumi, I Yanagisawa, K Katsurai, N Oka, N Tomonaga, H Tsutaya, H Kitao, A Neyama. Proc Waste Management 2000 in Tucson (CD-ROM), 2000.
4. CW Forsberg. Oak Ridge National Lab., Tenn., Report 4832000: 75, 2000.
5. K Munakata, S Yamatsuki, T Fukumatsu, K Tanaka. J Nucl Sci Technol 37: 84–89, 2000.
6. J Izumi. Chem Eng (Tokyo), 41: 557–563, 1996.
7. M Sazarashi, T Asami, K Akeshita, M Kumagai, T Tamura, Y Takashima. J Atom Energy Soc Jpn 34: 529–532, 1992.
8. T Kawai. Kouatsu Gasu [High Pressure Gas], 23: 8, 1986.
9. LP Geens, G Collard, W Goossens, L Baetsl. Radioact Waste Manag Nucl Fuel Cycle 6: 219–235, 1985.
10. H Ringel, R Printz. US DOE Rep., NUREG-CP-86-VOL-1: 566–577, 1987.
11. DT Pence, WJ Paplawsky. Proc 16th DOE Nuclear Air Cleaning Conference, 161, 1980.
12. H Fujiwara, T Murase, T Nishi, K Noshita, T Yoshida, M Matsuda. Mater Res Soc Proc 556: 375–382, 1999.
13. M Toyohara, M Kaneko. J Nucl Sci Technol 37: 970–978, 2000.
14. T Nakazawa. Scientific Basis for Nuclear Waste Management, 2000.
15. EC Moreno, M Kresak, RT Zahradnik. Nature 247: 64–65, 1974.
16. Y Kanda, Y Oki, M Numajiri, K Kondo. KEK Proc 13: 21–30, 2000.
17. J Izumi, H Tsutaya, A Ohmura, M Kubota, S Tooyama, M Hayano. Proc AIChE (Amer. Inst. Chem. Eng.) annual meeting (CD-ROM), 1999.
18. S Matsuoka, T Kodama, M Hatano, K Kurosu, H Anekawa, K Murasawa, A Yasutake, K Tokunaga, J Izumi. Abstr Atom Energy Soc Jpn spring meeting, 2002.
19. Fukumoto, M., Wada, R., Nishimura, T., Takeuchi, Y., Kurimoto, Y., Abstracts of the Atomic Energy Society of Japan Spring Meeting, 684, 2000.
20. CM Bethke. Geochemical Reaction Modeling. Oxford University Press, New York, 1996, p 397.
21. JR Martin. U.S. Patent 4,045,191.
22. J Izumi, S Tsubakizaki, T Morimoto, S Uchida. Japan Patent Tokukaihei 3-187416, 1993.